



Simulations of the instability of the $m=1$ self-shielding diocotron mode in finite-length nonneutral plasmas

Grant W. Mason and Ross L. Spencer

Citation: [AIP Conference Proceedings](#) **606**, 287 (2002); doi: 10.1063/1.1454295

View online: <http://dx.doi.org/10.1063/1.1454295>

View Table of Contents: <http://scitation.aip.org/content/aip/proceeding/aipcp/606?ver=pdfcov>

Published by the [AIP Publishing](#)

Articles you may be interested in

[Computing the \$m=1\$ diocotron frequency via an equilibrium calculation in non-neutral plasmas](#)

Phys. Plasmas **11**, 5356 (2004); 10.1063/1.1803840

[Nonlinear phase of the compressional \$m=1\$ diocotron instability: Saturation and analogy with geophysical fluid dynamics](#)

Phys. Plasmas **9**, 5059 (2002); 10.1063/1.1518473

[Simulations of the instability of the \$m=1\$ self-shielding diocotron mode in finite-length non-neutral plasmas](#)

Phys. Plasmas **9**, 3217 (2002); 10.1063/1.1488600

[\$l=1\$ diocotron instability of single charged plasmas in a cylindrical Penning trap with central conductor](#)

AIP Conf. Proc. **606**, 317 (2002); 10.1063/1.1454299

[The finite length diocotron mode](#)

Phys. Plasmas **5**, 601 (1998); 10.1063/1.872752

Simulations of the Instability of the $m = 1$ Self-Shielding Diocotron Mode in Finite-Length Nonneutral Plasmas

Grant W. Mason and Ross L. Spencer

Department of Physics and Astronomy, Brigham Young University, Provo, Utah 84602

Abstract. The “self-shielding” $m = 1$ diocotron mode in Malmberg-Penning traps has been known for over a decade to be unstable for finite length nonneutral plasmas with hollow density profiles. Early theoretical efforts were unsuccessful in accounting for the exponential growth and/or the magnitude of the growth rate. Recent theoretical work has sought to resolve the discrepancy either as a consequence of the shape of the plasma ends or as a kinetic effect resulting from a modified distribution function as a consequence of the protocol used to form the hollow profiles in experiments. We have investigated both of these finite length mechanisms in selected test cases using a three-dimensional particle-in-cell code that allows realistic treatment of shape and kinetic effects. We find that a persistent discrepancy of a factor of 2-3 remains between simulation and experimental values of the growth rate.

INTRODUCTION

Nonneutral plasmas, typically ions or electrons, can be confined for long periods of time in a cylindrical Malmberg-Penning trap similar to that shown in Fig. 1. A stiff axial magnetic field confines the particles radially, and charged rings at the ends of the otherwise grounded cylinder provide electrostatic longitudinal confinement. Diocotron modes are azimuthal drift waves in the cylindrical plasma that vary spatially as $\exp(im\theta)$. The theory of diocotron modes in nonneutral plasmas has its origins in seminal papers by Levy [1], Briggs, Daugherty and Levy [2], and the comprehensive treatment of nonneutral plasmas by Davidson [3].

The azimuthal mode of interest here occurs for hollow density profiles where the azimuthal flow of the plasma exhibits shear to create a rotation frequency profile $\omega_0(r)$ that rises with increasing radius from the center, peaks, then decreases to the wall. The resulting $m = 1$ mode (“self-shielded”) has a frequency near the peak of the frequency profile.

In the infinite length approximation, this mode is predicted not to be exponentially unstable for all radial density profiles of the plasma column. In contrast, when the plasma column is of finite length, the self-shielding $m = 1$ mode has been experimentally shown to be exponentially unstable for hollow density profiles [4, 5, 6].

Several theoretical attempts have been made to understand the origin of the instability [7, 8, 9, 10], but have failed to account for the exponential character of the stability and/or the size of the growth rate. In particular, Smith [8] has drawn attention to finite length effects and Finn *et al.* [11] have drawn attention to the importance of the shape

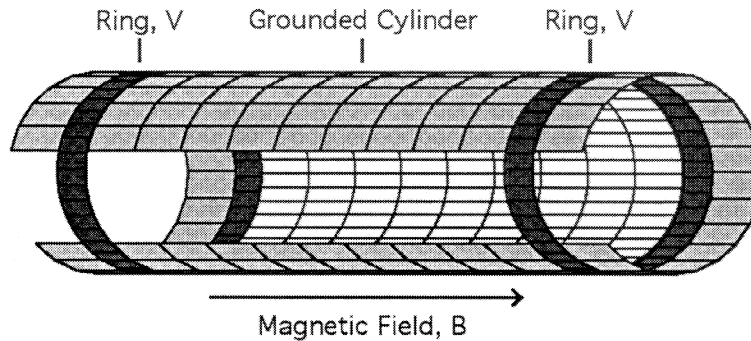


FIGURE 1. A Malmberg-Penning Trap. The axial magnetic field B confines charged particles radially and voltages V on the rings confine the nonneutral plasma longitudinally in the cavity space between the rings.

of the ends of the plasma based on an analogy to vortex stretching from topography variations in shallow fluid dynamics for geophysical flows. The theory of Finn, *et al.* when adapted to vortex dynamics in nonneutral plasmas, demonstrates that the radial variation of the equilibrium plasma length causes compression of the plasma parallel to the magnetic field while conserving the line integrated density. Their theory predicts the observed exponential growth of the instability, but predicts a growth rate that is still somewhat more than a factor of two less than a test case taken by Finn *et al.* [11] from data of Driscoll [5].

Coppa *et al.* [12] have refined the theory of Finn *et al.* but the refinements prove relatively small when applied to the test case of Finn *et al.*

Hilsabeck and O'Neil [13] develop a Zero Debye Length Reduced Description, but also fail to predict large enough growth rates based on end shape and length alone. However, they also observe that experimental procedures to produce plasmas with hollow profiles involve lowering the confining ring potentials and dumping preferentially the particles in the tail of the original Maxwellian velocity distribution, thus effectively truncating the velocity distribution near the center of the plasma. For certain distributions of axial energies, the instability can be substantially affected.

Here we report the results of three-dimensional particle-in-cell simulations that attempt to account for the remaining quantitative disagreement.

THEORY

We first consider electrons confined in cylindrical geometry by an axial magnetic field and an electrostatic potential. The equations describing the motion are isomorphic to those of two-dimensional fluid flow [1, 2] in the limit that the length of the plasma is much greater than its radius. In the case of the nonneutral plasma, the particles are considered to bounce longitudinally while drifting azimuthally. The bounce frequency is

taken to be much larger than the azimuthal $\mathbf{E} \times \mathbf{B}$ drift, so that the longitudinal dynamics is effectively separated from the bounce-averaged azimuthal drift. The fundamental equations of the Drift-Poisson Model then become (in the infinite length approximation),

$$\frac{\partial \rho}{\partial t} + \nabla \cdot (\rho \mathbf{u}) = 0 \quad \mathbf{u} = -\frac{\nabla \phi \times \hat{\mathbf{z}}}{B} \quad \nabla^2 \phi = -\frac{\rho}{\epsilon_0}. \quad (1)$$

The equations can be linearized assuming

$$\rho = \rho_0 + \rho_1 e^{i(m\theta - \omega t)} \quad \phi = \phi_0 + \phi_1 e^{i(m\theta - \omega t)} \quad \mathbf{u} = \mathbf{u}_0 + \mathbf{u}_1 e^{i(m\theta - \omega t)}, \quad (2)$$

leading to the diocotron mode equation,

$$(\omega - m\omega_0(r)) \left[\frac{1}{r} \frac{d}{dr} \left(r \frac{d}{dr} \phi_1 \right) - \frac{m^2 \phi_1}{r^2} \right] - \frac{mq}{\epsilon_0 B r} n'_0(r) \phi_1 = 0. \quad (3)$$

In the infinite length approximation, the self-shielding mode has frequency $\omega = \omega_0(r_{max})$ for which,

$$\phi_1 = r(\omega - \omega_0(r)), \quad r \leq r_{max} \quad (4)$$

$$\phi_1 = 0, \quad r > r_{max}, \quad (5)$$

where $\omega_0(r)$ is the equilibrium rotation frequency profile and r_{max} is the radius at which the profile peaks. The eigenfrequency is real and the mode is neutrally stable in this infinite length approximation.

Finn *et al.* identify two instability mechanisms when finite length plasma columns are considered. The first occurs when the shape of the end of the plasma is such that there is a radial variation of the equilibrium plasma length. In this case during motion there can be a compression of the plasma by the confining potential that conserves the line integrated density parallel to the magnetic field. The second mechanism is a perturbation of the plasma length when particles interact with the confining potential at the ends. Finn *et al.* demonstrate that both mechanisms give instability with comparable growth rates. The mode equation becomes [11],

$$\begin{aligned} (\omega - m\omega_0(r)) \left[\frac{1}{r} \frac{d}{dr} \left(r \frac{d}{dr} \phi_1 \right) - \frac{m^2 \phi_1}{r^2} \right] - m \frac{n'_0}{r} \phi_1 = \\ + \frac{mq}{\epsilon_0 B} \frac{n_0}{r} \frac{L'_0(r)}{L_0(r)} \phi_1 + \frac{q}{\epsilon_0} (\omega - m\omega_0(r)) n_0 \frac{\Lambda[\phi]}{L_0} \phi_1, \end{aligned} \quad (6)$$

where $L_0(r)$ and $L'_0(r)$ are respectively the equilibrium radial profile of the plasma length and its radial derivative. The functional $\Lambda[\phi]$ is the first order correction to the plasma length caused by perturbations in the potential [11]. To make the analysis tractable, Finn *et al.* approximate the equilibrium length of the plasma by a quadratic function. However, perturbations in the plasma length (Λ) were implemented ignoring curvature of the ends as a simple approximation.

The work of Hilsabeck and O’Neil and of Coppa *et al.* include refinements to the theory and implementation of Finn *et al.* Both accept an arbitrary plasma shape, use realistic axial boundary conditions, and incorporate perturbations in the plasma length self-consistently using a Green’s function. Solutions are by numerical methods. Both efforts find similar growth rates for the self-shielded mode that are several times smaller than the comparable test case taken from experiment. Calculated real frequencies of the mode are slightly smaller than the maximum of the rotation profile in contrast to experimental values that may be 25% lower than the maximum of the profile [13].

Hilsabeck and O’Neil conclude that quantitative agreement with the measured growth rates and frequencies requires the inclusion of a kinetic effect which arises from the experimental method used to load the hollow density profiles. The experimental protocol is assumed to truncate the high-velocity tails of the longitudinal velocity distribution in a radially dependent way. This can be important because the fast particles penetrate into a region in the ends of the plasma where their $\omega_0(r)$ is reduced compared to slower particles that do penetrate so deeply. If the longitudinal velocity distributions have radial dependence, the dynamics of the mode can be altered.

SIMULATIONS

In this paper we take a numerical approach by doing particle-in-cell simulations. The method has the advantage of incorporating realistic boundary and end conditions in detail while also providing diagnostic information about the plasmas that are otherwise unknown in the experiments or in the methods of Finn *et al.* and of Hilsabeck and O’Neil. We perform numerical experiments with the intent of helping to understand whether plasma shape and/or kinetic effects are adequate to predict experimentally measured growth rates for the unstable $m = 1$ diocotron mode in finite-length plasmas.

Azimuthally symmetric equilibria are computed separately using a two-dimensional ($r - z$) Successive Over-Relaxation (SOR) code [14]. Two-dimensional density and electric potential arrays are passed from the equilibrium code to the simulation code and interpolated onto a three-dimensional Cartesian grid. The three-dimensional density is then represented by particles-in-cells (PIC). The azimuthal symmetry of the distribution of particles is broken by small density perturbations or initial displacements of each particle chosen to seed a particular azimuthal mode using the infinite-length theory for the mode shapes.

In the present work, the plasma is typically represented by about 10^6 computational “particles” that, in turn, each represent several thousand plasma electrons. The computation is done in three-dimensional Cartesian geometry into which is embedded the confining cylinder. The grid used was $65 \times 65 \times 129$ for plasmas that were typically 0.30 m in length with a Debye length of ≥ 0.003 m. Short-legged differential operators for the Laplacian operator are used at the cylindrical boundary so that the cylindrical shape is treated realistically. Likewise, boundary conditions are implemented realistically, with a grounded cylinder sandwiched between confinement rings at each end held at sufficient potential to confine the plasma. Beyond the rings (longitudinally) and away from the plasma on each end is a short buffer zone of grounded cylinder at the end of

which periodic boundary conditions ($\partial\phi/\partial z = 0$) are maintained to complete the boundary conditions for the computation region.

Poisson's equation is solved by distributing density to the computational grid and using a three-dimensional multigrid algorithm to solve Poisson's Equation. Particles are moved in the (x, y) -plane assuming $\mathbf{E} \times \mathbf{B}$ drift motion and using a predictor-corrector algorithm. In the longitudinal z -direction we use Newton's Second Law and a leap-frog algorithm. Densities are distributed to the grid, fields are computed from Poisson's Equation, particles are moved in response to the fields, and new densities are computed to begin the cycle anew.

RESULTS

We have considered two "families" of equilibria. The first is based on a test case used by Finn *et al.* [11]. The electron plasma had a radius $r_p = 0.02$ m, confined within a cylinder of radius $r_w = 0.038$ m. The magnetic field was 375 G and the confining ring potentials were -50 V. The central cylinder had a length of 0.32 m. The rings had a width of 0.03 m and in this case the length of the buffer zone was zero.

The radial density profile of the plasma in the Finn theory was given by the parametrization,

$$n_0(r) = n_0(0)[1 - (r/r_p)^2]^2[1 + (\mu + 2)(r/r_p)^2] \quad (7)$$

for $r \leq r_p$ and zero elsewhere. The radial profile of the length of the plasma was parametrized by Finn *et al.* as

$$L_0(r) = L_0(0)[1 - \kappa(r/r_w)^2], \quad (8)$$

where r_w is the radius of the cylinder. The hollowness of the profile was controlled by the parameter μ and the curvature of the ends was described by the parameter κ . In the test case computed by Finn *et al.*, μ was chosen to be 3, resulting in a ratio $n_{max}/n_0 = 1.28$ and a value for κ of 0.25.

We prepared a simulation using the same radial density profile, plasma radius, cylinder radius, confining ring potentials and magnetic field as the Finn *et al.* test case. We chose a plasma temperature of 1.2 eV and a plasma length of 0.30 m. Under these conditions the value of kappa was approximately 0.3 and the value of n_{max} was 6.28×10^{12} particles per cubic meter corresponding to $\omega_0(max) = 1.44 \times 10^6 \text{ sec}^{-1}$. Plasma length profiles for the series of simulations based on the Finn *et al.* test case are shown in Fig. 2. Observe that the vertical scale is truncated. The radial variation of L_0 is relatively small compared to the overall length of the plasma. The profiles in Fig. 2 do not appear to be strictly parabolic, so our value of kappa (0.3) is only a rough approximation to the Finn value of 0.25.

At each time step of the simulation a longitudinally line-integrated density function was formed and then Fourier analyzed to find the amplitude and phase of the $m = 1$ mode. The phase signal as a function of time was used to measure the real frequency of the mode and an exponential function was fitted to the amplitude signal (as a function of time) to obtain the growth rate. The amplitude signal rises with an apparent exponential

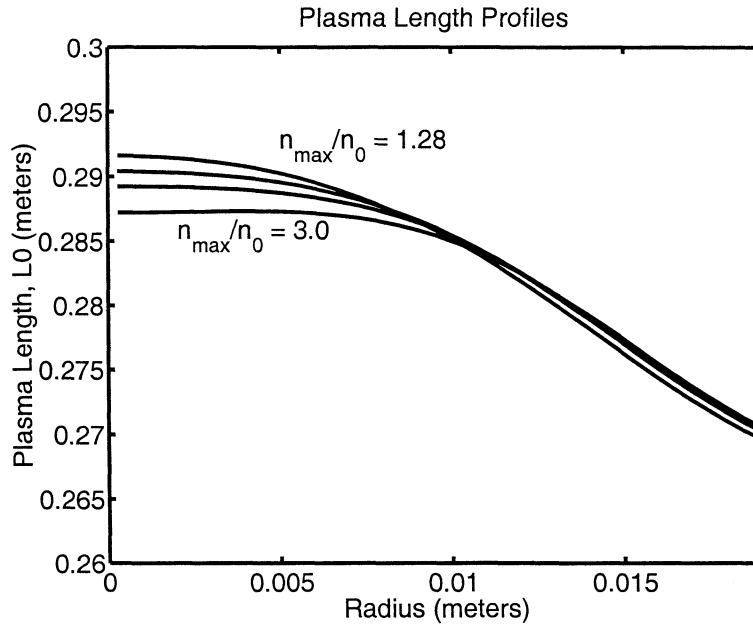


FIGURE 2. Radial length profiles for the plasmas identified with asterisks in Fig. 4. A parabolic fit ($L(x) = L_0(1 - \kappa(r/r_w)^2)$) to the uppermost curve yields roughly a value $\kappa = 0.3$. As n_{max}/n_0 increases, the profiles are less and less parabolic.

growth, but the signal wobbles slightly with time relative to the exponential. We have indicated with error bars an estimate of the uncertainty that this gave to the growth rate measurements. Figure 3 shows a typical amplitude signal with a corresponding exponential growth for comparison as well as the corresponding phase signal.

The results of the simulations are shown in Fig. 4. The ratio of growth rate to real mode frequency is about 0.007 compared to the Finn *et al.* result of 0.009, the Coppa *et al.* result of 0.008, and the experimental value of 0.025. Our real frequency was $1.40 \times 10^6 \text{ sec}^{-1}$ which is consistent with the expectation of a real frequency near the maximum of the radial rotation profile of our equilibrium ($1.44 \times 10^6 \text{ sec}^{-1}$). In each case in Fig. 4, the simulation gives a real frequency of the mode to within 1-3% of the maximum of the rotation profile $\omega_0(\text{max})$.

We completed the first “family” of simulations by maintaining the value of $n_0(\text{max})$ and deepening the profile using the Finn *et al.* radial density parameterization with $\mu = 5.66, 8.19, 15.07$. The corresponding ratios n_{max}/n_0 are 1.64, 2.00, 3.00. These growth rates are also shown in Fig. 4 as the points marked with the asterisk (*) symbol. The point at $n_{max}/n_0(0) = 2$ is coincident with the prediction of our drift-kinetic code.

The second family of simulations was done to address the possibility suggested by Hilsabeck and O’Neil that the persistent discrepancy between experiment and theory may be a kinetic effect when particles of differing energies penetrate the confining potential at the ends to differing degrees. This effect may be enhanced because, experimen-

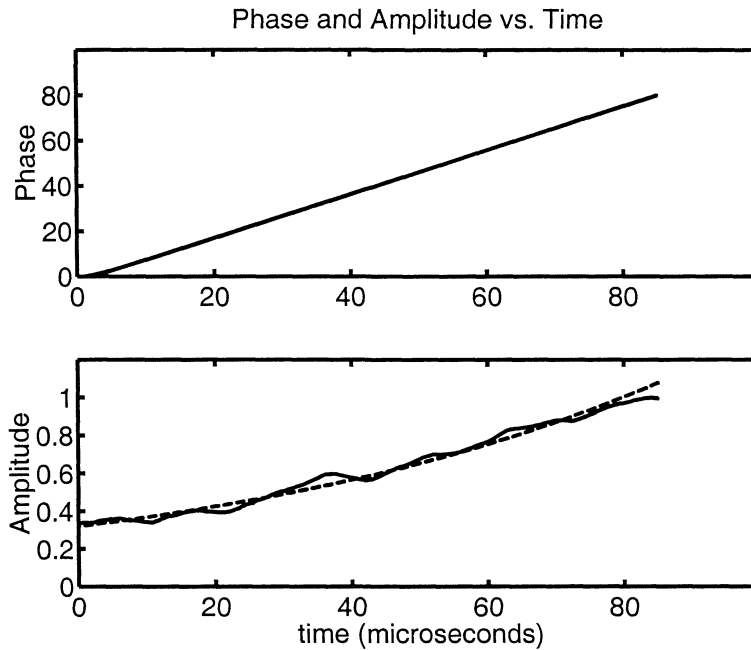


FIGURE 3. (Upper) The phase signal in radians from which the real frequency ω_r of the mode is determined. The phase signal from the simulation is remarkably linear. (Lower) An exponential growth curve compared to the amplitude signal for the $m = 1$ mode from the particle-in-cell simulations. Error flags on the simulation results plotted in Fig. 4 are estimates of the uncertainty in growth rate determinations based on figures like this one.

tally, the hollow profiles are created from a non-hollow profile by temporarily lowering the end potentials. This procedure allows more particles to escape near $r = 0$ than at larger radii, but also depletes the Maxwellian distribution of velocities in a radially dependent way. The nonmaxwellian distributions created in this way will depend heavily on the protocol used to create the plasmas and experimental velocity distribution data are not available for a specific test case.

For purposes of simulation, we began with a flat-topped density profile. We again used a magnetic field of 375 G and a temperature of 1.2 eV. However, the radius of the cylinder was 0.05 m and the plasma length about 0.35 m. The central density plateau was 5×10^{12} per cubic meter. The confining ring potentials were -200 V. The central cylinder had a length of 0.44 m, rings a width of 0.03 m, and a buffer zone length of 0.05 m.

The equilibrium was calculated and loaded into the simulation code as before. However, when the code began, the ring voltages (boundary conditions) were reduced linearly over a 1 μsec period of time to some fraction of the original confining value chosen to reduce the potential near $r = 0$ to a value close to the central potential of the plasma. The rings were then held down at this destination potential for 4 μsec , then linearly raised

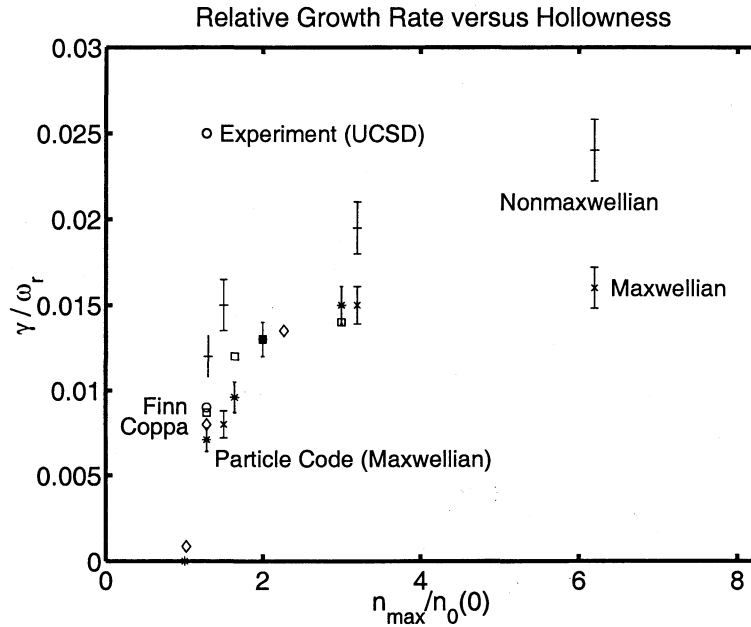


FIGURE 4. Comparisons of calculated growth rates to the theory of Finn *et al.* and an experimental test case (open circles). Asterisks (*) mark simulation points based on a test case of Finn *et al.* taken from experiment (UCSD). Hyphens (-) mark simulation points obtained by depleting the tails of the longitudinal velocity distributions. Corresponding Maxwellian cases are marked by “x” for comparison. Also included for comparison are predictions from our drift-kinetic code calculation (open boxes) and results of the “complete model” of Coppa *et al.* marked with diamonds.

again to the original value over a final microsecond. The resulting density profile was hollow and not unlike the profiles obtained from the Finn *et al.* formula. The degree of hollowness ($n_{max}/n_0(0)$) was controlled by the fraction applied to the -200 V ring potentials when the confining potentials were lowered. Since the potential remained down for several bounce times, virtually all particles with longitudinal velocities below a certain critical value were removed. The velocity distributions resulting from this protocol had a radial dependence and since equilibration times were much longer than the time of our simulation, the resulting velocity distributions as a function of radius were and remained “nonmaxwellian” through the course of the simulation. The hollowed density profiles created in this way are shown in Fig. 5. Figure 6 shows the corresponding root-mean-square velocity profiles.

Three plasmas were created using the protocol described above with $n_{max}/n_0 = 1.5, 3.2, 6.2$. The corresponding density profiles are shown in Fig. 5. The growth rates are shown in Fig. 4 marked with the hyphen (-) symbol. The 6.2 point is labelled as “nonmaxwellian.” For comparison, we took the radial density profiles from these three nonmaxwellian simulations and created distributions differing only in that the longitudinal velocity distributions were Maxwellian at all radii (with temperature 1.2

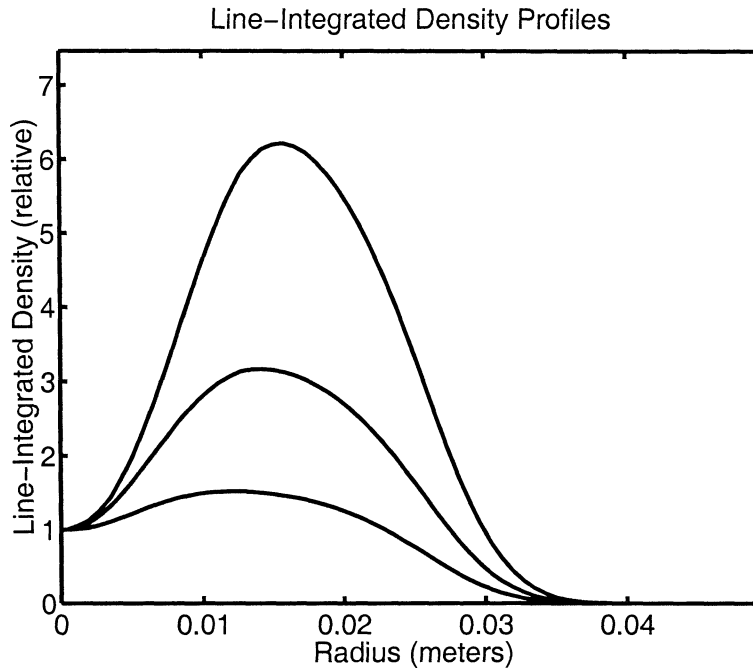


FIGURE 5. Simulated hollow line-integrated density profiles obtained by temporarily lowering the potentials on the confinement rings according to the protocol described in the text. Absolute line integrated densities at $r = 0$ are 1.10×10^{12} (bottom), 5.12×10^{11} (middle), and 2.52×10^{11} (top) particles per square meter.

eV). These are shown in Fig. 4 marked with the “x” symbol. The nonmaxwellian growth rates are enhanced over their Maxwellian counterparts by factors of 1.9, 1.3, and 1.5 for n_{max}/n_0 equal to 1.5, 3.2, and 6.2 respectively.

As an approximate check of the results of our simulations and to provide an additional comparison to results by Finn *et al.* and Coppa *et al.*, we have used a separate linear drift-kinetic eigenvalue code to compute growth rates. The code, which was originally written for the infinitely-long plasma approximation, was easily modified to include the L'_0/L_0 term on the right-hand-side of Eq. 6 but not the Λ term. The eigenvalue code uses equilibria calculated separately by the same SOR code used to calculate equilibria for the simulations using density profiles from Eq. 7. See Fig. 4.

This independent calculation reproduces the Finn *et al.* growth rate almost exactly at $n_{max}/n_0 = 1.28$, coincides exactly with the simulation point at $n_{max}/n_0 = 1.64$, and meshes smoothly with the results of Coppa *et al.* using their “complete model.” The results of our eigenvalue code are shown as open squares in Fig. 4. The results of Coppa *et al.* are shown as open diamonds.

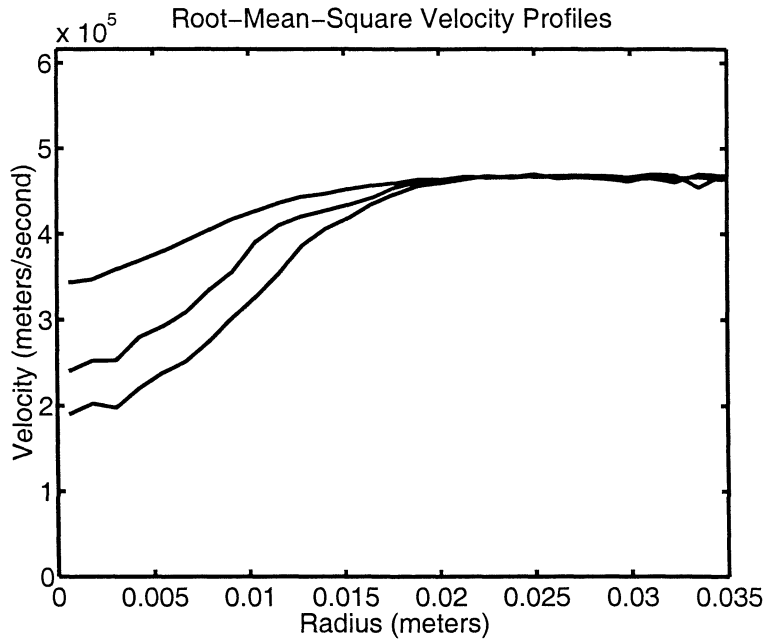


FIGURE 6. Radial root-mean-square velocity (v_z) profiles for the simulated plasmas of Fig. 5. The corresponding velocity distributions at each radius are identified as “nonmaxwellian” in Fig. 4.

CONCLUSIONS

We have used particle-in-cell simulations to compute growth rates for the hollow, finite-length $m = 1$ self-shielded diocotron mode. We have investigated test cases where the persistent discrepancy between theory and experiment may be a consequence of the shape of the ends of the plasma or kinetic effects arising from a nonmaxwellian velocity distributions introduced in the experimental preparation of the plasmas. In none of the test families were we able to achieve growth rates as large as the experimental value. Real frequencies computed in the simulations for the self-shielding mode were typically within about 3% of the maxima of the respective rotation profiles. Thus, we agree with the conclusion of Hilsabeck and O’Neil that the end shape effects we considered are alone insufficient to remove the discrepancy with experiment.

We have also simulated a nonmaxwellian longitudinal velocity distribution effect suggested by Hilsabeck and O’Neil. The effect increases growth rates by 30-90% compared to Maxwellian control cases. Nevertheless, the simulation is still a factor of 2.0 too low to remove the discrepancy with experiment at $n_{max}/n_0(0) = 1.28$. However, the two methods which we used to create the nonmaxwellian distributions may not correspond to the actual experimental protocols, leaving some room yet for further study.

ACKNOWLEDGEMENTS

We gratefully acknowledge helpful discussions with J. M. Finn, D. del Castillo-Negrete, T. M. O'Neil, D. H. E. Dubin, T. J. Hilsabeck, and A. A. Kabantsev. S. N. Rasband provided helpful results from a recently-developed cold-fluid code against which we compared test runs from the PIC code described in this paper. We also gratefully acknowledge the use of facilities of the Brigham Young University Supercomputing Center.

REFERENCES

1. R. H. Levy, *Phys. Fluids* **8**, 1288 (1965); **11**, 920 (1968).
2. R. J. Briggs, J. D. Daugherty, and R. H. Levy, *Phys. Fluids* **13**, 421 (1970).
3. R. C. Davidson, *Theory of Nonneutral Plasmas* (Benjamin, Reading, MA, 1974).
4. C. F. Driscoll and K. S. Fine, *Phys. Fluids B* **2**, 1359 (1990).
5. C. F. Driscoll, *Phys. Rev. Lett.* **64**, 645 (1990).
6. A. Kabantsev and C. Driscoll, in *Non-Neutral Plasmas III*, edited by J. Bollinger, R. Spencer, and R. Davidson (American Institute of Physics, New York, 1999), pp. 208-213.
7. R. A. Smith and M. N. Rosenbluth, *Phys. Rev. Lett.* **64**, 649 (1990).
8. R. A. Smith, *Phys. Fluids B* **4**, 287 (1992).
9. S. N. Rasband, R. L. Spencer, and R. R. Vanfleet, *Phys. Fluids B* **5**, 669 (1993).
10. S. N. Rasband, *Phys. Plasmas* **3**, 94 (1996).
11. J. M. Finn, D. del Castillo-Negrete, and D. C. Barnes, *Phys. Plasmas* **6**, 3744 (1999).
12. G. G. M. Coppa, A. D'Angola, G. L. Delzanno, and G. Lapenta, *Phys. Plasmas* **8**, 1133 (2001).
13. T. J. Hilsabeck and T. M. O'Neil, *Phys. Plasmas* **8**, 407 (2001).
14. R. L. Spencer, S. N. Rasband, and R. R. Vanfleet, *Phys. Fluids B*, **5**, 1738 (1993).